JCI insight

**Amendment history:**
- Erratum (September 2020)

# TFEB-driven lysosomal biogenesis is pivotal for PGC1α-dependent renal stress resistance

Matthew R. Lynch, … , Toren Finkel, Samir M. Parikh

*JCI Insight.* 2019. https://doi.org/10.1172/jci.insight.126749.

Research In-Press Preview Nephrology

## Graphical abstract

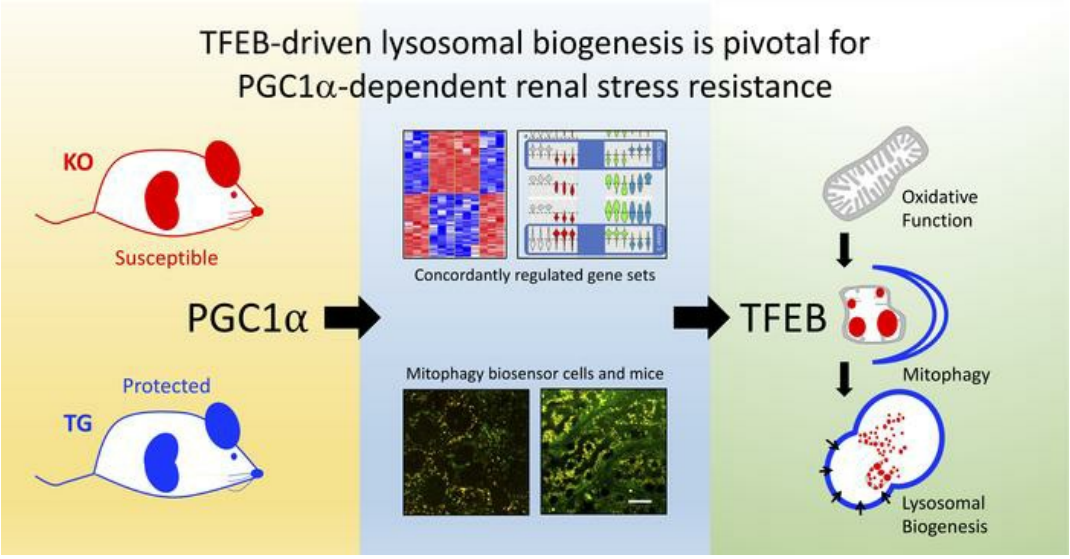


## Find the latest version:

https://jci.me/126749/pdf

# TFEB-driven lysosomal biogenesis is pivotal for PGC1α-dependent renal stress resistance

Matthew R. Lynch[#,1,2], Mei T. Tran[#,1,2], Kenneth M. Ralto[#,1,2], Zsuzsanna K. Zsengeller[3], Vinod Raman[1,2], Swati S. Bhasin[2], Nuo Sun[4], Xiuying Chen[1,2], Daniel Brown[3], Ilsa I. Rovira[4], Kensei Taguchi[5], Craig R. Brooks[5], Isaac E. Stillman[3], Manoj K. Bhasin[2], Toren Finkel[4,6], Samir M. Parikh[1,2]

[#]These authors contributed equally to the work

[1]Division of Nephrology, Beth Israel Deaconess Medical Center and Harvard Medical School, Boston MA
[2]Department of Medicine, Beth Israel Deaconess Medical Center and Harvard Medical School, Boston MA
[3]Department of Pathology, Beth Israel Deaconess Medical Center and Harvard Medical School, Boston, MA
[4]Center for Molecular Medicine, National Heart, Lung and Blood Institute, NIH, Bethesda, MD
[5]Division of Nephrology and Hypertension, Department of Medicine, Vanderbilt University Medical Center, Nashville, TN
[6]Aging Institute of UPMC and the University of Pittsburgh, Pittsburgh, PA

Correspondence:
Samir Parikh
Beth Israel Deaconess Medical Center
330 Brookline Ave, RN 330C
Boston, MA 02215

Email: sparikh1@bidmc.harvard.edu

**Publication Fees/Creative Commons License:**

Conduct of this work and fees for publication are supported by grants from the National Institutes of Health. NIH Public Access Policy therefore applies to this submission.

https://publicaccess.nih.gov/faq.htm#753

**Conflict of Interest statement**

SMP is listed as an inventor on a related patent filed by Beth Israel Deaconess Medical Center.

**ABSTRACT**

Because injured mitochondria can accelerate cell death through the elaboration of oxidative free radicals and other mediators, it is striking that proliferator gamma coactivator 1-alpha (PGC1α), a stimulator of increased mitochondrial abundance, protects stressed renal cells instead of potentiating injury. Here we report that PGC1α's induction of lysosomes via transcription factor EB (TFEB) may be pivotal for kidney protection. CRISPR and stable gene transfer showed that PGC1α knockout tubular cells were sensitized to the genotoxic stressor cisplatin whereas transgenic cells were protected. The biosensor mtKeima unexpectedly revealed that cisplatin blunts mitophagy both in cells and mice. PGC1α not only counteracted this effect but also raised basal mitophagy, as did the downstream mediator nicotinamide adenine dinucleotide (NAD+). PGC1α did not consistently affect known autophagy pathways modulated by cisplatin. Instead RNA sequencing identified coordinated regulation of lysosomal biogenesis via TFEB. This effector pathway was sufficiently important that inhibition of TFEB or lysosomes unveiled a striking harmful effect of excess PGC1α in cells and conditional mice. These results uncover an unexpected effect of cisplatin on mitophagy and PGC1α's exquisite reliance on lysosomes for kidney protection. Finally, the data illuminate TFEB as a novel target for renal tubular stress resistance.

## INTRODUCTION

Mitochondria are critical for normal kidney function, evidenced by the high penetrance of tubulopathy among people with monogenic mitochondrial diseases (1). Yet, mitochondria also amplify injury responses to diverse stressors including ischemia and inflammation (2-4). The injured mitochondrion promotes cell death by producing excessive free radicals and other pro-apoptotic mediators (4, 5). Thus, while mitochondria enable life-sustaining functions, they also accelerate cell death when stressed.

From this perspective, increased mitochondrial abundance prior to injury should favor cell death rather than cell protection. Yet, we recently found that tubular induction of the mitochondrial biogenesis factor PGC1$\alpha$ increased mitochondrial mass and also protected from ischemic and inflammatory renal injury (6). Kang and colleagues similarly observed tubular PGC1$\alpha$-dependent kidney protection in a model of crystal nephropathy (7). In the brain, PGC1$\alpha$ limits the damage that can arise from mitochondrial oxidants by inducing antioxidant enzymes (8). However, renal tubular PGC1$\alpha$ does not induce such enzymes (6), leaving unaddressed how mitochondrial biogenesis and mitochondrially-targeted antioxidants can both be beneficial in the same models of AKI.

These studies were initiated to ask whether PGC1$\alpha$-dependent renoprotection extends to toxic AKI, a heretofore unaddressed question. A combination of novel genetic cellular models, genetic mouse models, cellular and murine biosensor studies, and unbiased profiling yielded unanticipated insights regarding PGC1$\alpha$-dependent mitochondrial quality control mechanisms in the renal tubule; our understanding of cisplatin nephrotoxicity; and TFEB as a new target for renal stress resistance.

## RESULTS

We created stable loss-of-function renal tubular cells to study PGC1$\alpha$ by CRISPR (**Supplemental Figure 1**) and stable PGC1$\alpha$ transgenic counterparts by lentiviral gene transfer (**Supplemental Figure 2**). The cells exhibited expected changes in cellular respiration (**Supplemental Figure 3**). For both the canonical mitochondrial biogenesis function of PGC1$\alpha$ and the more recently described induction of NAD+ biosynthesis (6, 9), these cells paralleled kidney expression patterns of PGC1$\alpha$ knockout (KO) and Pax8-rtTA x tetO-PGC1$\alpha$ conditional tubular transgenic (hereafter iNephPGC1$\alpha$) mice (**Figure 1A,**

**B**). After completing concentration-ranging studies in cells (**Supplemental Figure 4A**), we found that KO cells produced baseline less adenosine triphosphate (ATP) and suffered greater ATP depletion following cisplatin than control cells (**Figure 1C, D**). Conversely, PGC1α transgenic cells produced more baseline ATP and preserved ATP following cisplatin (**Figure 1E, F**). Viability assays were analogous: KO cells were more susceptible to cisplatin whereas transgenic cells were more resistant (**Figure 1G, H**). Given these concordant results, we tested different doses of cisplatin in mice (**Supplemental Figure 4B**), then treated PGC1α KO mice and iNephPGC1α mice with cisplatin. The former developed worse acute kidney injury (AKI) as assessed by the filtration marker serum creatinine, whereas the latter were more resistant to cisplatin than respective controls (**Figure 1I-N**). Cisplatin-mediated injury to tubules was also quantified by the expression of kidney injury molecule-1 (KIM1) in renal homogenates from these experiments (**Supplemental Figure 5**). These studies confirmed the effects of PGC1α gene modulation observed on cisplatin cytotoxicity in vitro and nephrotoxicity in vivo. Together, these results establish the utility of KO and transgenic cells as models of tubular PGC1α. They show for the first time that PGC1α is required for resistance to cisplatin nephrotoxicity. Furthermore, forced tubular PGC1α is sufficient to promote resistance against this stressor. Finally, the salutary action of renal tubular PGC1α is cell-autonomous.

Earlier literature has reported that cisplatin augments autophagy (10, 11). Consistent with this concept, we found that levels of the autophagic marker p62 rose after cisplatin (**Supplementary Figure 6**). However, there was neither a robust nor concordant effect of PGC1α manipulation on p62. Cisplatin also increased PTEN-induced kinase protein 1 (PINK1), a mediator of mitophagy recently implicated in cisplatin toxicity (12-15). However, PGC1α did not exert a concordant effect on PINK1 in this setting (**Supplementary Figure 7**). To address further how cisplatin has been reported to induce these clearance mechanisms, yet induction of such mechanisms also counteracts toxicity (16, 17), we next visualized mitophagy by stably expressing the biosensor mtKeima in PGC1α KO and transgenic cells (18-20). This dual-fluorescent probe reports the pH shift as basic mitochondria undergo mitophagy in acidic lysosomes (**Figure 2 schematic**). In contrast to a recent report (14), the data with mtKeima suggested that cisplatin decreased mitophagy in renal tubular cells (**Supplemental Figure 8**). Furthermore, in PGC1α KO cells, basal mitophagy was decreased and cisplatin exacerbated this (**Figure 2A-M**). In PGC1α transgenic cells, mitophagy was preserved despite cisplatin (**Figure 2N**). Biosensor studies therefore uncovered new effects both of cisplatin and renal tubular PGC1α. Given the concordant effects on metabolism, viability and mitophagy—i.e., cisplatin reduces, PGC1α depletion exacerbates, and PGC1α induction ameliorates—we tested augmentation of NAD+, an

emerging mimetic of PGC1α's renal effects with translational potential (6, 21). Application of the precursor nicotinamide mononucleotide (NMN) restored mitophagy in cisplatin-treated PGC1α KO cells (**Figure 2O**). Transgenic mtKeima mice verified that cisplatin reduced renal tubular mitophagy, an effect NMN counteracted (**Figure 3**).

With unexpected evidence of (A) cisplatin reducing mitophagy and (B) PGC1α counteracting this effect without (C) impacting known cisplatin-dependent mechanisms, we conducted RNA sequencing to seek a mechanistic link by exploiting the symmetry of cisplatin's effects in PGC1α KO and transgenic cells. Unsupervised hierarchical clustering confirmed intra-group homogeneity and inter-group "distance" between KO and transgenic cells (**Figure 4A**). Supervised differential and self-organizing maps (SOM) analysis isolated transcripts whose expression was oppositely regulated by PGC1α KO vs. transgenic status (clusters 2 and 5 in **Figure 4B**). Among these was TFEB (**Figure 4C**), a master regulator of lysosomal biogenesis and autophagy (22). In neurons, PGC1α induces TFEB to counteract proteotoxicity (23). In nematodes, TFEB and PGC1α are mutually regulatory (24). Both a previously described TFEB-dependent gene set (25) and a curated database of genes involved in lysosomal biology (http://lysosome.unipg.it) were significantly over-represented ($p < 0.05$) among PGC1α-oppositely regulated transcripts (**Supplemental Figure 9**). PGC1α KO exacerbated whereas PGC1α induction ameliorated cisplatin's suppressive effect on TFEB (**Figure 4D-G**). Even absent cisplatin, lysosomal abundance mirrored PGC1α's effects on TFEB: decreased in KO and increased in transgenic cells relative to controls (**Figure 4H, I**). When cisplatin was applied, lysosomal abundance decreased, an effect NMN again counteracted (**Figure 4J**).

This emerging concept suggested both a novel tubular protection mechanism via TFEB and a way to reconcile how PGC1α enhances stress resistance even as it adds potentially noxious mitochondrial mass. We therefore hypothesized that impairment of lysosomes would unmask a toxic effect of PGC1α related to mitochondrial injury. Cisplatin-treated PGC1α transgenic cells were indeed ***more*** susceptible to TFEB depletion than cisplatin-treated controls (**Figure 5A-E**). TFEB depletion fully ***reversed*** the suppressive effect of PGC1α on mitochondrial reactive oxygen species induced by cisplatin (**Figure 5F**). Electron microscopy of cisplatin-treated PGC1α KO mouse kidneys showed mitochondrial damage whereas iNephPGC1α kidneys displayed abundant lysosomes and autolysosomes sequestering swollen mitochondria (**Figure 5G-N**). Mirroring TFEB knockdown results, the lysosome inhibitor chloroquine now ***exacerbated*** cisplatin nephrotoxicity iNephPGC1α mice (**Figure 5O**). And cisplatin-

treated iNephPGC1α mice displayed ***increased*** oxidative stress (**Figure 5P,Q**). Finally, iNephPGC1α mice exhibited enlarged lysosomes and autolysosomes (**Supplementary Figure 10**).

## DISCUSSION

The combination of loss- and gain-of-PGC1α—both in cells and in mice—provide consistent, powerful evidence that PGC1α in the renal tubular epithelium critically affects metabolic, cellular, and physiological responses to toxic injury. Together with published inflammatory and post-ischemic AKI models (6, 26), the data are notably concordant: starting with less PGC1α worsens unrelated forms of acute renal tubular injury whereas starting with more PGC1α affords protection.

The present results mechanistically elucidate how PGC1α benefits stressed renal tubular epithelial cells without exposing those cells to the downside risks of noxious potentiators that emanate from injured mitochondria such as mitochondria-derived free radicals. In non-renal models, diverse extra-mitochondrial PGC1α effectors have been implicated (27-29). In the case of neuronal PGC1α, these effectors include anti-oxidant enzymes that can detoxify mitochondrial free radicals (8). In contrast to these results outside of the kidney, renal tubular PGC1α defends mitochondrial energy extraction even during stress (6, 7, 26, 30, 31) and without the induction of anti-oxidant enzymes (6). The gain-of-function mouse model employed herein increases renal tubular mitochondrial abundance ***before*** the onset of injury (6, 7), raising questions about how the renal tubule is spared from mitochondrial oxidants once cisplatin is administered (32). Our data propose that PGC1α acts via TFEB to accelerate mitochondrial turnover. During injury, this may enable efficient and safe disposal of damaged mitochondria, thereby limiting intracellular exposure to oxidants emanating from damaged mitochondria. Coupled with its mitochondrial biogenesis function, the net effect of PGC1α in the stressed renal tubule may be to shift the distribution of mitochondria toward healthier organelles with better energy extraction and less free radical production. The PGC1α pathway is so strongly reliant on TFEB and lysosomes that its effect during stress flips from protection to harm depending on these effectors' status. This two-fold action of PGC1α—lysosomes curtailing mitochondrial oxidants plus healthier mitochondria defending ATP production—may thus be central to its wide-ranging renoprotection.

We recently reported that PGC1α induces a biosynthetic pathway for cells to increase the co-enzyme NAD+ (6, 21). As the chief electron acceptor from glycolysis and the tricarboxylic acid cycle, sole electron donor to Complex I of the electron transport chain, and a requisite substrate for metabolism-modifying sirtuin enzymes, it is perhaps unsurprising that intracellular NAD+ levels have been reported to be rate-limiting for oxidative metabolism (33). For highly oxidative cells, this means that a reduction in NAD+ translates into less efficient mitochondrial function and thus less ATP. During AKI, renal NAD+ levels decline because PGC1α-dependent NAD+ biosynthesis falls and because NAD+ consumption rises due to stress-induced enzymes such as poly-ADP ribose polymerases (PARPs) (6, 34). Consistent with this body of results, administration of PGC1α-independent NAD+ precursor compounds ameliorates different forms of experimental AKI as shown here and previously (6). The present results further show that NAD+ augmentation mimics PGC1α's effects on mitophagy. While the exact mechanisms linking NAD+ to mitophagy need to be elucidated, the literature suggests two intriguing possibilities. First, as a substrate for sirtuins, NAD+ has been shown to promote PGC1α deacetylation, a post-translational modification that increases PGC1α's transcriptional co-activator function (35). Thus NAD+ is on one hand a downstream product of PGC1α, but on the other, an upstream activator of the protein. Alternatively, sirtuins can activate a coordinated transcriptional response to mitochondrial stress known as the mitochondrial unfolded protein response ($UPR^{mt}$) (36). The $UPR^{mt}$ may operate in parallel or in an overlapping fashion with mitophagy to restore healthy organellar function. Since the molecular links between $UPR^{mt}$ and mitophagy have been elusive (37), future studies with cisplatin may yield new insights.

Multiple studies offer the apparent dueling perspectives that cisplatin increases autophagy and mitophagy, yet promotion of these processes counteracts its toxicity (38). The present data endorse a new synthesis. Mitophagy may be induced early after cisplatin, but as an adaptive rather than toxic response. By a later time closer to overt kidney dysfunction, cisplatin may retard this process, thereby accelerating cell death (11). Our cellular results at 24h of exposure and in vivo results 72h after cisplatin suggest that cisplatin ultimately impedes mitophagy. Because mtKeima reports a shift to acidic pH in the environment of mitochondria, our results cannot distinguish whether mitophagy is blunted at the step of mitochondrial uptake into autophagosomes or post-uptake acidification as this unit matures into a degradative autolysosome (or both). Despite this limitation, the results support a model in which effective mitochondrial clearance is blunted following cisplatin. The late failure to maintain adaptive clearance mechanisms could be a proximate cause of cell death and account for the delayed rise in serum creatinine that characterizes the clinical syndrome of cisplatin nephrotoxicity. Detailed autophagy and mitophagy flux studies are needed to illuminate the kinetics of this process.

TFEB may be a new target in AKI. Monogenic lysosomal diseases illustrate how important safe waste disposal is for human renal health (39). Termed the CLEAR network (Coordinated Lysosomal Expression And Regulation), TFEB's gene targets link early steps of autophagy to lysosomal biogenesis to drive an integrated program for cellular waste removal (40, 41). We found that PGC1α is required for intact renal tubular TFEB expression, that more PGC1α further induces TFEB, and that TFEB is required for PGC1α-dependent tubular protection. In the liver, TFEB promotes PGC1α transcription by directly ligating its promoter, and, may in turn, be upregulated by one of PGC1α's canonical transcription factor partners, PPARα (24). Such reciprocal regulation between PGC1α and TFEB may also be present in the renal tubule. Consequently, therapeutic TFEB activation during AKI could help break a vicious cycle triggered by injury-induced suppression of PGC1α (26). Development of small molecule TFEB agonists should enable studies in genetic models and acquired forms of PGC1α deficiency. Careful investigation of TFEB agonists at multiple time points may also elucidate the time window in which lysosomes are most important to combat cisplatin's toxic renal effects. Conversely, the exciting prospect that PGC1α could modulate chronic lysosomal diseases affecting the kidney should be tested.

In summary, the present results address a continuum of mitochondrial homeostasis in the injured kidney spanning the production and disposal of these organelles; identify blunted mitophagy as a novel effect of cisplatin; define PGC1α as a determinant of renoprotection against cisplatin; and implicate TFEB as a new mediator of renal stress resistance. These results could have future impact on the treatment of common acute and rare renal diseases.

## METHODS

### Creation of PGC1α KO cell lines

PGC1α knockout cells were created from an immortalized mouse inner medullary collecting duct cell line (mIMCD-3, ATCC). The CRISPR/Cas9 system used to knock out PGC1α was described by Ran, et al (42). LentiCRISPR v2 was a gift from Feng Zhang (Addgene plasmid # 52961) (43). The sgRNA sequence used to target the mouse PGC1α coding sequence was 5'-CCGCTCGGATTTCCTGGTCT-3'. Successfully transfected cells were selected using puromycin. Single cell colonies of selected cells were created using the clonal dilution method. Clones were validated by sequencing the region flanking the sgRNA target sequence and by biochemical assays as described. A control cell line was created in parallel with a control sgRNA that was non-complementary to any mouse genomic sequence.

### Creation of PGC1α transgenic cell lines

PGC1α transgenic cells were created by transduction of mIMCD-3 cells with a 3rd generation lentiviral transfer plasmid expressing the mouse PGC1α open reading frame. Cells were co-transfected using the psPAX2 packaging plasmid and the pMD2.G envelope plasmid. pLenti CMV GFP Puro (658-5) was a gift from Eric Campeau & Paul Kaufman (Addgene plasmid # 17448) (44). GFP-PGC1α was a gift from Bruce Spiegelman (Addgene plasmid # 4) (45). psPAX2 was a gift from Didier Trono (Addgene plasmid # 12260). pMD2.G was a gift from Didier Trono (Addgene plasmid # 12259). Lentiviral particles were created by transfection of HEK293T cells and subsequently concentrated using the Lenti-X concentrator (Clontech). Transfected cells were selected with the addition of puromycin to complete media at 1μg/mL. Transgenic cells were validated by confirming PGC1α overexpression using real-time quantitative PCR. Transgenic control cells were created in parallel which contained an empty lentiviral expression vector and were also maintained in puromycin-containing media.

### Viability and ATP assays

Cell viability was assessed using an XTT assay (ATCC). ATP measurements were determined with a luminescent kit (Abcam). Mitochondrial reactive oxygen species in cells were determined by MitoSOX assay per manufacturer's instructions (ThermoFisher Scientific). Cells were transfected with siRNA targeting mouse TFEB or a negative control siRNA (ThermoFisher Scientific) for 72h.

### Oxygen consumption experiments

Cells were seeded in an XF 24-well cell culture plate (Seahorse Bioscience) at $4 \times 10^4$ cells per well and grown in complete medium. Prior to oxygen consumption analysis, media was changed to

Seahorse XF Base Medium (Seahorse Bioscience) supplemented with 1mM pyruvate, 10 mM glucose, 1 mM pyruvate and adjusted to pH 7.4. Oxygen consumption rates (pmol/min) were assessed using an XF-24 Flux Analyzer (Seahorse Bioscience) at baseline, after the addition of the ATP synthase inhibitor oligomycin (1 μM), after the addition of the uncoupling agent 2,4-dinitrophenol (1 μM), and again after addition of the complex I inhibitors rotenone (0.5 μM) and antimycin A (0.5 μM).

**Western analysis**

Cell lysate preparation, gel electrophoresis, transfer, immunoblotting, detection, and image acquisition were performed as previously described (6, 26). Antibodies used were TFEB (Bethyl Labs, A303-673A) and p62 (Sigma-Aldrich, P0067).

**Mitophagy and lysosomal measurements**

Detailed methods for the measurement of mitophagy based on mitochondrial-targeted Keima have been described previously (19, 20). Briefly, fluorescence of mtKeima was imaged in two channels via two sequential excitations (458 nm, “green” and 561 nm, “red” respectively) and using a 570-695 nm emission range by live confocal microscopy (Zeiss). A mitophagy index was calculated by determining the ratio between the area of the red (acidic) and green (basic) emission. For mitophagy index calculation in mtKeima mice, the average of four images from each tissue sample was taken and the values were normalized to the average value seen in the controls, assigned the value of one. In each experimental model, all imaging parameters remained the same for all data acquisition using Zen Zeiss software. Acidified lysosomes were labeled using Lysotracker Red DND-99 (ThermoFisher Scientific) and imaged at an excitation/emission of 577/590 nm using live confocal microscopy.

**RNA sequencing and Bioinformatics**

Poly(A)-enriched RNA was isolated from PGC1$\alpha$ KO and Tg cells and their respective genotype controls (described above) treated with cisplatin 10$\mu$M for 24h. Three replicates were collected per condition and checked for quality on denaturing agarose gel. Sequencing libraries were generated from double-stranded cDNA using the Illumina TruSeq kit according to the manufacturer’s instructions. Library quality was checked using the Agilent DNA High Sensitivity Chip and qRT-PCR. High-quality libraries were then sequenced on an Illumina NextSeq 2000. To achieve comprehensive coverage for each sample, approximately 25-30 million paired-end reads were generated. Raw results were passed through quality control steps and aligned to the mouse genome. Gene expression determinations were performed from aligned reads by counting unique reads. Read-count-based expression data were normalized by the voom method, which estimates the mean variance relationship of log-counts and

assigns a weight to each observation prior to linear modeling. Normalized count data were compared between groups using a linear modeling approach by implementing Limma R package to identify differentially expressed genes based on multiple-test-corrected P value and fold change (46). To extract patterns in genes that were significantly altered (multiple tested corrected P-value < 0.05 and absolute fold change > 2) in PGC1α KO and Tg cells, self-organizing maps (SOM) analysis was performed (26). For example, Clusters 2 and 5 indicated gene sets oppositely regulated in the test conditions—either elevated in KO and depressed in Tg or depressed in KO and elevated in Tg. This gene set was then evaluated for over-representation of genes described in Settembre, et al., (25) or against a curated database of genes involved in lysosomal biology (http://lysosome.unipg.it) by applying the Fisher's exact test. Sequencing data have been uploaded at https://www.ncbi.nlm.nih.gov/geo/ under GSE126259.

**Mouse studies**

Tubule-specific PGC1α conditionally overexpressing transgenic (Pax8-rtTA x tetO-PGC1α, referred to as iNephPGC1α or Tg mouse), PGC1α knockout (KO), and mtKeima mice have been previously described (6, 20, 26). Each parent strain was obtained from Jackson Labs where extensive details on strain background are available: Pax8-rtTA (stock #007176); tetO-PGC1α (stock #012387); PGC1α KO (stock #008597); and mtKeima (stock #028072). Experiments were performed on male mice ages 8-11 weeks old using littermate controls by an operator blinded to genotype and randomized within each cage to vehicle vs. AKI model.

Cisplatin, nicotinamide mononucleotide, and chloroquine were purchased from Sigma Aldrich. All treatments administered to mice were given by intraperitoneal injection. Cisplatin treatment was 20mg/kg for PGC1α KO and mtKeima mice; 30mg/kg for iNephPGC1α Tg mice. These doses were based on previous literature (47) and informed by published guidance from the United States Food and Drug Administration (FDA) as described below. Nicotinamide mononucleotide (NMN, 400 mg/kg) was given 24h and 1h prior to cisplatin, followed by a final dose at 24h after cisplatin treatment. Chloroquine (10 mg/kg) was given 1h prior to cisplatin, then every 24h until sacrifice (48). Serum and organs from all cisplatin-treated mice were collected and analyzed at 72h. Creatinine from mouse serum was measured using LC/MS-MS at the University of Alabama Birmingham O'Brien Core Center for Acute Kidney Injury Research in a blinded fashion (NIH P30 DK079337).

A typical human dose of cisplatin is 60mg/$m^2$ intravenously per cycle. For a 60 kg individual with height 65 inches, this calculates to 100mg—i.e., 1.67mg/kg. Per guidance from the FDA (link below), this human dose in mg/$m^2$ can be scaled to mouse dose in mg/kg either by dividing the human dose by 3 (60mg/$m^2$ for human / 3 = 20mg/kg for mouse) or by converting the human dose into mg/kg then multiplying by 12.3 (1.67mg/kg for human * 12.3 = 20.5mg/kg for mouse).

(https://www.fda.gov/downloads/Drugs/Guidances/UCM078932.pdf%23search=%27guidekines+for+industry+sfe+starting%27)

**Quantitative PCR**

Total RNA extraction and cDNA synthesis were performed as previously described (6). PCR reactions were performed in duplicate using QuantStudio 6 Flex Real-Time PCR System (Applied Biosystems). SYBR primers were designed using PrimerQuest Tool (Integrated DNA Technologies). Relative expression levels were determined using the comparative threshold method. Measured transcripts included genes involved in PGC1$\alpha$-dependent mitochondrial biogenesis (TFAM = transcription factor A mitochondrial, ATP5O = ATP synthase subunit O mitochondrial, and NDUFS1 = NAD-ubiquinone oxidoreductase 75kDa subunit mitochondrial); and genes involved in PGC1$\alpha$-dependent NAD+ biosynthesis (IDO2 = indole dioxygenase 2, AFMID = arylformamidase, QPRT = quinolinate phosphoribosyl transferase, NADSYN1 = NAD synthetase 1, and NAMPT = nicotinamide phosphoribosyltransferase) (6, 9).

**Structured Illumination Microscopy**

Paraffin embedded kidney tissue was sectioned at 4-6 $\mu$m and mounted on silanized ((3-Aminopropyl) trimethoxysilane, Sigma Aldrich) cover glass (limited working distances for super resolution objectives necessitates mounting the tissue directly to the coverslip). Antigen retrieval was carried out by incubating the sections in 0.1M citrate buffer at high temperature (115$^{o}$C) and high pressure using a pressure cooker. Tissues were blocked with normal donkey serum and stained with anti-LAMP2 (Abcam, clone GL2A7) and anti-LC3 (NanoTools, Clone 5F10, Biotinylated) antibodies. Donkey anti-Rat Cy3 secondary (Jackson ImmunoResearch, catalog # 712-166-153) was used to detect anti-LAMP2 and Streptavidin DyLight 488 (Invitrogen, catalog # 21832) was used to detect anti-LC3. Nuclei were stained with DAPI (Sigma). Tissues were imaged on a N-SIM microscope (Nikon structured illumination microscope) using a 100x TIRF super-resolution objective and taken as a z-stack at 0.12 $\mu$m/z step. The resulting z-stack was processed in Imaris software (Bitplane, Concord MA) to generate 3D surface renderings and graphs of rendered structures. SIM imaging and image processing was

performed in part through the use of the Vanderbilt Cell Imaging Shared Resource and Nikon Center of Excellence (supported by NIH grants CA68485, DK20593, DK58404, DK59637 and EY08126).

**Electron microscopy**

The complete method is previously described (32, 49). Briefly, kidneys were fixed with 2.5% glutaraldehyde in 0.1 M cacodylate buffer (pH 7.4) and cut in 1μm sections in both sagittal and transverse planes for image analysis. After drying the sections, slides were stained at 65$^{o}$C for 20 minutes in 0.1% Toluidine blue in 1% sodium borate, cooled to room temperature, washed in distilled water, cleaned in xylene, and mounted in Permount sections for light microscopy. Subsequent ultrathin sections (0.5 μm) were examined by transmission electron microscopy (JEOL 1011, JEOL Corp.) with Orca-HR Digital Camera (Hamamatsu Corp.), and Advanced Microscopy Technique Corporation image capture system.

**Statistics**

For all studies, non-parametric tests were used to compare continuous variables (Mann-Whitney U test or Kruskal Wallis if > 2 groups) unless otherwise noted. Two-factor ANOVA was employed for grouped analyses with p-values corrected for multiple comparisons as appropriate. Data are presented as mean ± SEM unless otherwise specified. Power for mouse studies was guided by the following calculation from pilot studies of cisplatin nephrotoxicity: serum creatinine of 0.8 ± 0.3 mg/dl in wildtype mice vs. 1.5 ± 0.5 mg/dl in PGC1α KO mice requires seven mice per group for > 90% power. Mouse AKI models were performed by an operator (MTT) blinded to genotype and with random assignment to control vs. injury condition. Serum creatinine was measured by a core service indicated above that was blinded to experimental conditions. Histopathology and ultrastructure were evaluated by operators (ZKZ and IES) blinded to condition. Results were prepared using Graphpad Prism Version 7 (La Jolla, CA). Two-tailed p-values < 0.05 were considered significant. *p<0.05, **p< 0.01, ***p<0.001, ****p< 0.0001 unless otherwise indicated.

**Study Approval**

Mouse studies were conducted with approval by the Institutional Animal Care and Use Committee (IACUC) at Beth Israel Deaconess Medical Center (Boston, MA) and the National Heart Lung Blood Institute (Bethesda, MD).

## AUTHOR CONTRIBUTIONS

MRL conducted cellular studies focused on autophagy and mitophagy measurements. MTT conducted cellular studies with siTFEB and mouse studies with assistance from XC. KMR developed and characterized stable KO and transgenic cells for PGC1$\alpha$. ZKZ, DB, and IES conducted histopathological studies on mouse tissues. SSB and MKB analyzed RNA sequencing results. NS, IIR, and TF studied mtKeima transgenic mice. CRB and KT conducted structured illumination microscopy studies on kidneys from PGC$\alpha$ genetic models treated with cisplatin. MTT, MRL, KMR, and SMP prepared the manuscript with input from all authors.

**ACKNOWLEDGMENTS**

The authors thank researchers at Beth Israel Deaconess Medical Center for fruitful discussions. Pilot studies were presented at the 2018 American Society of Nephrology Kidney Week. SMP's laboratory is supported by R01-DK095072, R35-HL139424, and R01-AG1027002. CRB and KT are supported by K01DK099473 and P30 DK114809.

## REFERENCES


1. Emma F, Montini G, Parikh SM, and Salviati L. Mitochondrial dysfunction in inherited renal disease and acute kidney injury. *Nature reviews Nephrology.* 2016;12(5):267-80.
2. Mills EL, Kelly B, Logan A, Costa ASH, Varma M, Bryant CE, et al. Succinate Dehydrogenase Supports Metabolic Repurposing of Mitochondria to Drive Inflammatory Macrophages. *Cell.* 2016;167(2):457-70 e13.
3. West AP, Brodsky IE, Rahner C, Woo DK, Erdjument-Bromage H, Tempst P, et al. TLR signalling augments macrophage bactericidal activity through mitochondrial ROS. *Nature.* 2011;472(7344):476-80.
4. Chouchani ET, Pell VR, Gaude E, Aksentijevic D, Sundier SY, Robb EL, et al. Ischaemic accumulation of succinate controls reperfusion injury through mitochondrial ROS. *Nature.* 2014;515(7527):431-5.
5. Balaban RS, Nemoto S, and Finkel T. Mitochondria, oxidants, and aging. *Cell.* 2005;120(4):483-95.
6. Tran MT, Zsengeller ZK, Berg AH, Khankin EV, Bhasin MK, Kim W, et al. PGC1alpha drives NAD biosynthesis linking oxidative metabolism to renal protection. *Nature.* 2016;531(7595):528-32.
7. Kang HM, Ahn SH, Choi P, Ko YA, Han SH, Chinga F, et al. Defective fatty acid oxidation in renal tubular epithelial cells has a key role in kidney fibrosis development. *Nature medicine.* 2015;21(1):37-46.
8. St-Pierre J, Drori S, Uldry M, Silvaggi JM, Rhee J, Jager S, et al. Suppression of reactive oxygen species and neurodegeneration by the PGC-1 transcriptional coactivators. *Cell.* 2006;127(2):397-408.
9. Wu Z, Puigserver P, Andersson U, Zhang C, Adelmant G, Mootha V, et al. Mechanisms controlling mitochondrial biogenesis and respiration through the thermogenic coactivator PGC-1. *Cell.* 1999;98(1):115-24.
10. Yang C, Kaushal V, Shah SV, and Kaushal GP. Autophagy is associated with apoptosis in cisplatin injury to renal tubular epithelial cells. *American journal of physiology Renal physiology.* 2008;294(4):F777-87.
11. Periyasamy-Thandavan S, Jiang M, Wei Q, Smith R, Yin XM, and Dong Z. Autophagy is cytoprotective during cisplatin injury of renal proximal tubular cells. *Kidney international.* 2008;74(5):631-40.
12. Wang Y, Tang C, Cai J, Chen G, Zhang D, Zhang Z, et al. PINK1/Parkin-mediated mitophagy is activated in cisplatin nephrotoxicity to protect against kidney injury. *Cell Death Dis.* 2018;9(11):1113.
13. Ichinomiya M, Shimada A, Ohta N, Inouchi E, Ogihara K, Naya Y, et al. Demonstration of Mitochondrial Damage and Mitophagy in Cisplatin-Mediated Nephrotoxicity. *Tohoku J Exp Med.* 2018;246(1):1-8.
14. Zhao C, Chen Z, Xu X, An X, Duan S, Huang Z, et al. Pink1/Parkin-mediated mitophagy play a protective role in cisplatin induced renal tubular epithelial cells injury. *Exp Cell Res.* 2017;350(2):390-7.
15. Zhao C, Chen Z, Qi J, Duan S, Huang Z, Zhang C, et al. Drp1-dependent mitophagy protects against cisplatin-induced apoptosis of renal tubular epithelial cells by improving mitochondrial function. *Oncotarget.* 2017;8(13):20988-1000.
16. Jiang M, Wei Q, Dong G, Komatsu M, Su Y, and Dong Z. Autophagy in proximal tubules protects against acute kidney injury. *Kidney international.* 2012;82(12):1271-83.
17. Herzog C, Yang C, Holmes A, and Kaushal GP. zVAD-fmk prevents cisplatin-induced cleavage of autophagy proteins but impairs autophagic flux and worsens renal function. *American journal of physiology Renal physiology.* 2012;303(8):F1239-50.

18. Katayama H, Kogure T, Mizushima N, Yoshimori T, and Miyawaki A. A sensitive and quantitative technique for detecting autophagic events based on lysosomal delivery. *Chem Biol.* 2011;18(8):1042-52.
19. Sun N, Malide D, Liu J, Rovira, II, Combs CA, and Finkel T. A fluorescence-based imaging method to measure in vitro and in vivo mitophagy using mt-Keima. *Nat Protoc.* 2017;12(8):1576-87.
20. Sun N, Yun J, Liu J, Malide D, Liu C, Rovira, II, et al. Measuring In Vivo Mitophagy. *Mol Cell.* 2015;60(4):685-96.
21. Poyan Mehr A, Tran MT, Ralto KM, Leaf DE, Washco V, Messmer J, et al. De novo NAD(+) biosynthetic impairment in acute kidney injury in humans. *Nature medicine.* 2018;24(9):1351-9.
22. Settembre C, Fraldi A, Medina DL, and Ballabio A. Signals from the lysosome: a control centre for cellular clearance and energy metabolism. *Nat Rev Mol Cell Biol.* 2013;14(5):283-96.
23. Tsunemi T, Ashe TD, Morrison BE, Soriano KR, Au J, Roque RA, et al. PGC-1alpha rescues Huntington's disease proteotoxicity by preventing oxidative stress and promoting TFEB function. *Science translational medicine.* 2012;4(142):142ra97.
24. Settembre C, De Cegli R, Mansueto G, Saha PK, Vetrini F, Visvikis O, et al. TFEB controls cellular lipid metabolism through a starvation-induced autoregulatory loop. *Nat Cell Biol.* 2013;15(6):647-58.
25. Settembre C, Di Malta C, Polito VA, Garcia Arencibia M, Vetrini F, Erdin S, et al. TFEB links autophagy to lysosomal biogenesis. *Science.* 2011;332(6036):1429-33.
26. Tran M, Tam D, Bardia A, Bhasin M, Rowe GC, Kher A, et al. PGC-1alpha promotes recovery after acute kidney injury during systemic inflammation in mice. *J Clin Invest.* 2011;121(10):4003-14.
27. Arany Z, Foo SY, Ma Y, Ruas JL, Bommi-Reddy A, Girnun G, et al. HIF-independent regulation of VEGF and angiogenesis by the transcriptional coactivator PGC-1alpha. *Nature.* 2008;451(7181):1008-12.
28. Patten IS, Rana S, Shahul S, Rowe GC, Jang C, Liu L, et al. Cardiac angiogenic imbalance leads to peripartum cardiomyopathy. *Nature.* 2012;485(7398):333-8.
29. Lin J, Wu PH, Tarr PT, Lindenberg KS, St-Pierre J, Zhang CY, et al. Defects in adaptive energy metabolism with CNS-linked hyperactivity in PGC-1alpha null mice. *Cell.* 2004;119(1):121-35.
30. Han SH, Malaga-Dieguez L, Chinga F, Kang HM, Tao J, Reidy K, et al. Deletion of Lkb1 in Renal Tubular Epithelial Cells Leads to CKD by Altering Metabolism. *Journal of the American Society of Nephrology : JASN.* 2016;27(2):439-53.
31. Han SH, Wu MY, Nam BY, Park JT, Yoo TH, Kang SW, et al. PGC-1alpha Protects from Notch-Induced Kidney Fibrosis Development. *Journal of the American Society of Nephrology : JASN.* 2017.
32. Zsengeller ZK, Ellezian L, Brown D, Horvath B, Mukhopadhyay P, Kalyanaraman B, et al. Cisplatin nephrotoxicity involves mitochondrial injury with impaired tubular mitochondrial enzyme activity. *J Histochem Cytochem.* 2012;60(7):521-9.
33. Bai P, Canto C, Brunyanszki A, Huber A, Szanto M, Cen Y, et al. PARP-2 regulates SIRT1 expression and whole-body energy expenditure. *Cell metabolism.* 2011;13(4):450-60.
34. Ebrahimkhani MR, Daneshmand A, Mazumder A, Allocca M, Calvo JA, Abolhassani N, et al. Aag-initiated base excision repair promotes ischemia reperfusion injury in liver, brain, and kidney. *Proceedings of the National Academy of Sciences of the United States of America.* 2014;111(45):E4878-86.
35. Rodgers JT, Lerin C, Haas W, Gygi SP, Spiegelman BM, and Puigserver P. Nutrient control of glucose homeostasis through a complex of PGC-1alpha and SIRT1. *Nature.* 2005;434(7029):113-8.
36. Mouchiroud L, Houtkooper RH, Moullan N, Katsyuba E, Ryu D, Canto C, et al. The NAD(+)/Sirtuin Pathway Modulates Longevity through Activation of Mitochondrial UPR and FOXO Signaling. *Cell.* 2013;154(2):430-41.

37. Shpilka T, and Haynes CM. The mitochondrial UPR: mechanisms, physiological functions and implications in ageing. *Nature reviews Molecular cell biology.* 2018;19(2):109-20.
38. Havasi A, and Dong Z. Autophagy and Tubular Cell Death in the Kidney. *Semin Nephrol.* 2016;36(3):174-88.
39. Najafian B, Fogo AB, Lusco MA, and Alpers CE. AJKD Atlas of Renal Pathology: Fabry nephropathy. *Am J Kidney Dis.* 2015;66(5):e35-6.
40. Sardiello M, Palmieri M, di Ronza A, Medina DL, Valenza M, Gennarino VA, et al. A gene network regulating lysosomal biogenesis and function. *Science.* 2009;325(5939):473-7.
41. Palmieri M, Impey S, Kang H, di Ronza A, Pelz C, Sardiello M, et al. Characterization of the CLEAR network reveals an integrated control of cellular clearance pathways. *Hum Mol Genet.* 2011;20(19):3852-66.
42. Ran FA, Hsu PD, Wright J, Agarwala V, Scott DA, and Zhang F. Genome engineering using the CRISPR-Cas9 system. *Nature protocols.* 2013;8(11):2281.
43. Sanjana NE, Shalem O, and Zhang F. Improved vectors and genome-wide libraries for CRISPR screening. *Nature methods.* 2014;11(8):783-4.
44. Campeau E, Ruhl VE, Rodier F, Smith CL, Rahmberg BL, Fuss JO, et al. A versatile viral system for expression and depletion of proteins in mammalian cells. *PLoS One.* 2009;4(8):e6529.
45. Puigserver P, Wu Z, Park CW, Graves R, Wright M, and Spiegelman BM. A cold-inducible coactivator of nuclear receptors linked to adaptive thermogenesis. *Cell.* 1998;92(6):829-39.
46. Smyth GK. Linear models and empirical bayes methods for assessing differential expression in microarray experiments. *Stat Appl Genet Mol Biol.* 2004;3:Article3.
47. Brooks C, Wei Q, Cho SG, and Dong Z. Regulation of mitochondrial dynamics in acute kidney injury in cell culture and rodent models. *J Clin Invest.* 2009;119(5):1275-85.
48. Mei S, Livingston M, Hao J, Li L, Mei C, and Dong Z. Autophagy is activated to protect against endotoxic acute kidney injury. *Sci Rep.* 2016;6:22171.
49. Mukhopadhyay P, Horvath B, Zsengeller Z, Zielonka J, Tanchian G, Holovac E, et al. Mitochondrial-targeted antioxidants represent a promising approach for prevention of cisplatin-induced nephropathy. *Free Radic Biol Med.* 2012;52(2):497-506.

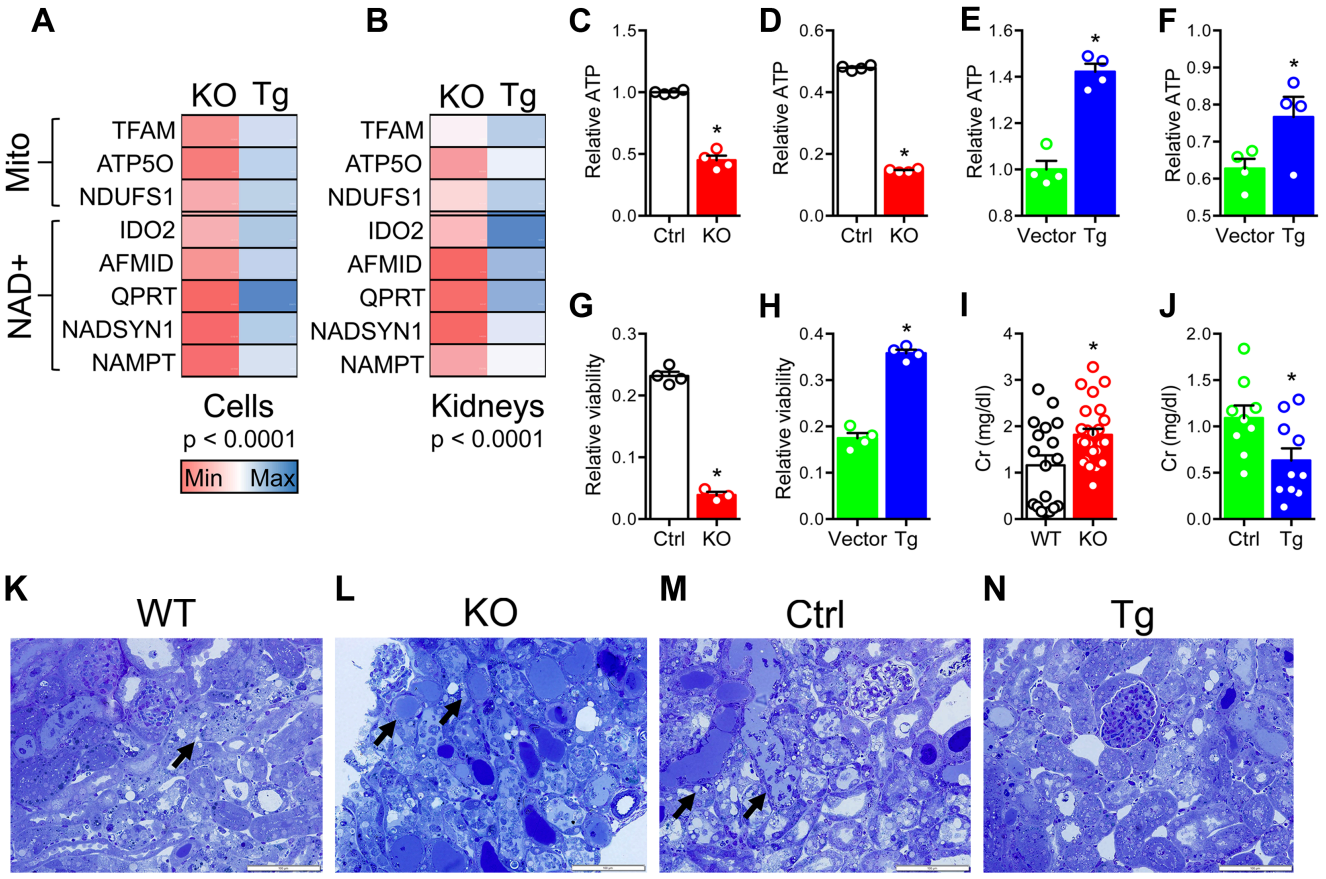


**Figure 1: Loss- or gain-of-PGC1α confers concordant effects against cisplatin toxicity in cells and in mice.** (A, B) Heatmaps comparing mitochondrial and NAD+ biosynthetic enzyme expression patterns of PGC1α knockout (KO) vs. transgenic renal tubular cells and renal expression in KO mice vs. iNephPGC1α (Tg) mice. Each cell represents average expression scaled to respective control (n=3-6/group). Multiple comparison p-values by ANOVA. Gene abbreviations defined in Methods. (C,D) ATP abundance in Ctrl and PGC1α KO cells at baseline (C) and after cisplatin (D, 10μM, 24h). Data in D normalized to Ctrl cells at baseline. (E,F) ATP abundance in Vector and PGC1α Tg cells at baseline (E) and after cisplatin (F, 10μM, 24h). Data in F normalized to Vector cells at baseline. (G,H) Viability via XTT assay after cisplatin (10μM, 24h). Results normalized to respective controls at baseline. N= 4/group for C-H. (I,J) Serum creatinine (Cr, mg/dl) in PGC1α KO mice (I, n=18 WT vs. 25 KO mice) or iNephPGC1α (J, n=9 Ctrl vs. 10 Tg mice) 72h after cisplatin (20 mg/kg intraperitoneal in PGC1α KO and 30 mg/kg in iNephPGC1α) vs. respective controls. (K-N) Toluidine-blue stained plastic sections of renal cortex from (representative of 3-4 mice from I,J) with black arrows to necrotic tubules. Scale bars 100μm. *p<0.05 by Mann-Whitney for C-J.

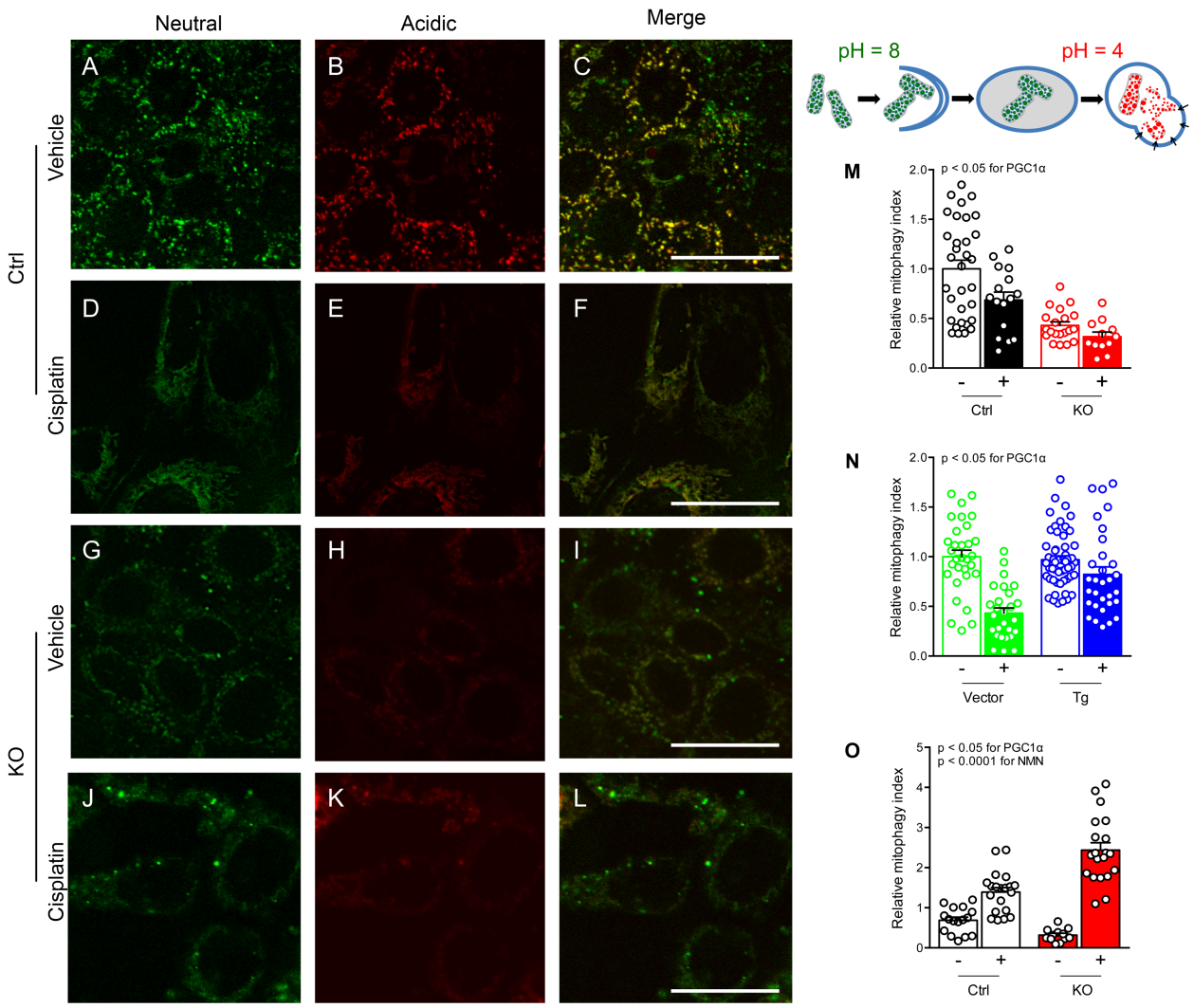


**Figure 2: Cisplatin reduces mitophagy which PGC1α counteracts.** *(top right)* Color shift in mtKeima indicates mitophagy from green (neutral) to red (acidic). (A-L) PGC1α KO cells or controls treated with vehicle or cisplatin (10μM, 24h). Scale bar 5μm. (M) Quantification of mitophagy index for (A-L) relative to control condition. N=32, 16, 20, and 12 fields left to right from 3-4 biological replicates per condition. (N) Mitophagy index for PGC1α Tg cells or vector controls treated with vehicle or cisplatin (10μM, 24h). N=31, 27, 54, and 31 fields left to right from 3-6 biological replicates per condition. (O) PGC1α KO cells treated with cisplatin (10μM, 24h) ± concurrent nicotinamide mononucleotide (NMN, 1mM). N=16, 20, 12, and 20 fields left to right from 3-4 biological replicates per condition. Results analyzed by two-way ANOVA on biological replicates with p-values as indicated.

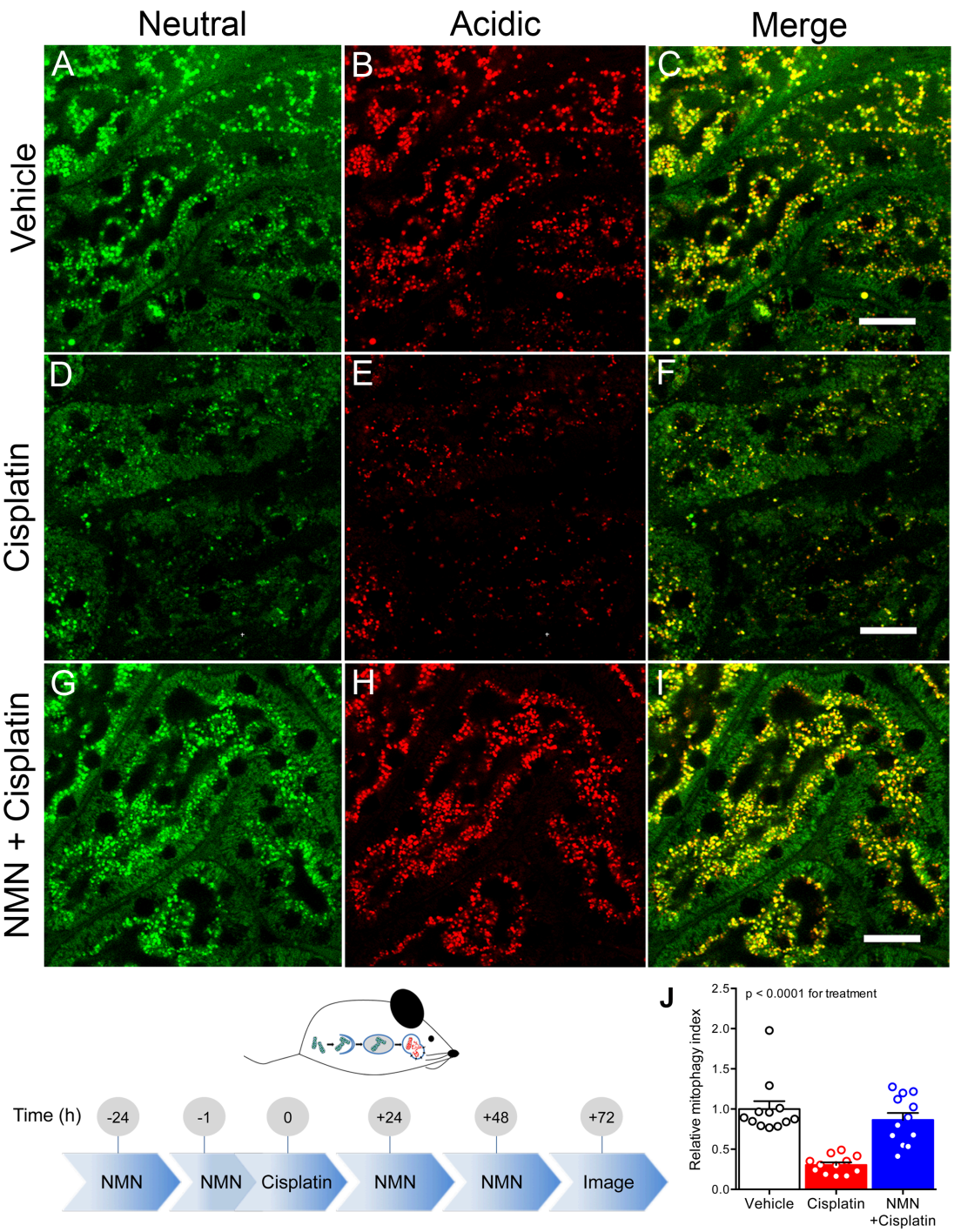


**Figure 3: Cisplatin reduces mitophagy in vivo which NMN counteracts.** *(bottom left)* Schematic depicting experimental interventions in mtKeima transgenic mice. (A-I) Renal cortex of mtKeima mice treated with vehicle or cisplatin (20mg/kg intraperitoneal, 72h) ± NMN (400mg/kg intraperitoneal as indicated). Scale bar 50μm. (J) Quantification of mitophagy index for (A-I) relative to control condition. N=12 fields from 3 mice per condition. P-value calculated by ANOVA on biological replicates.

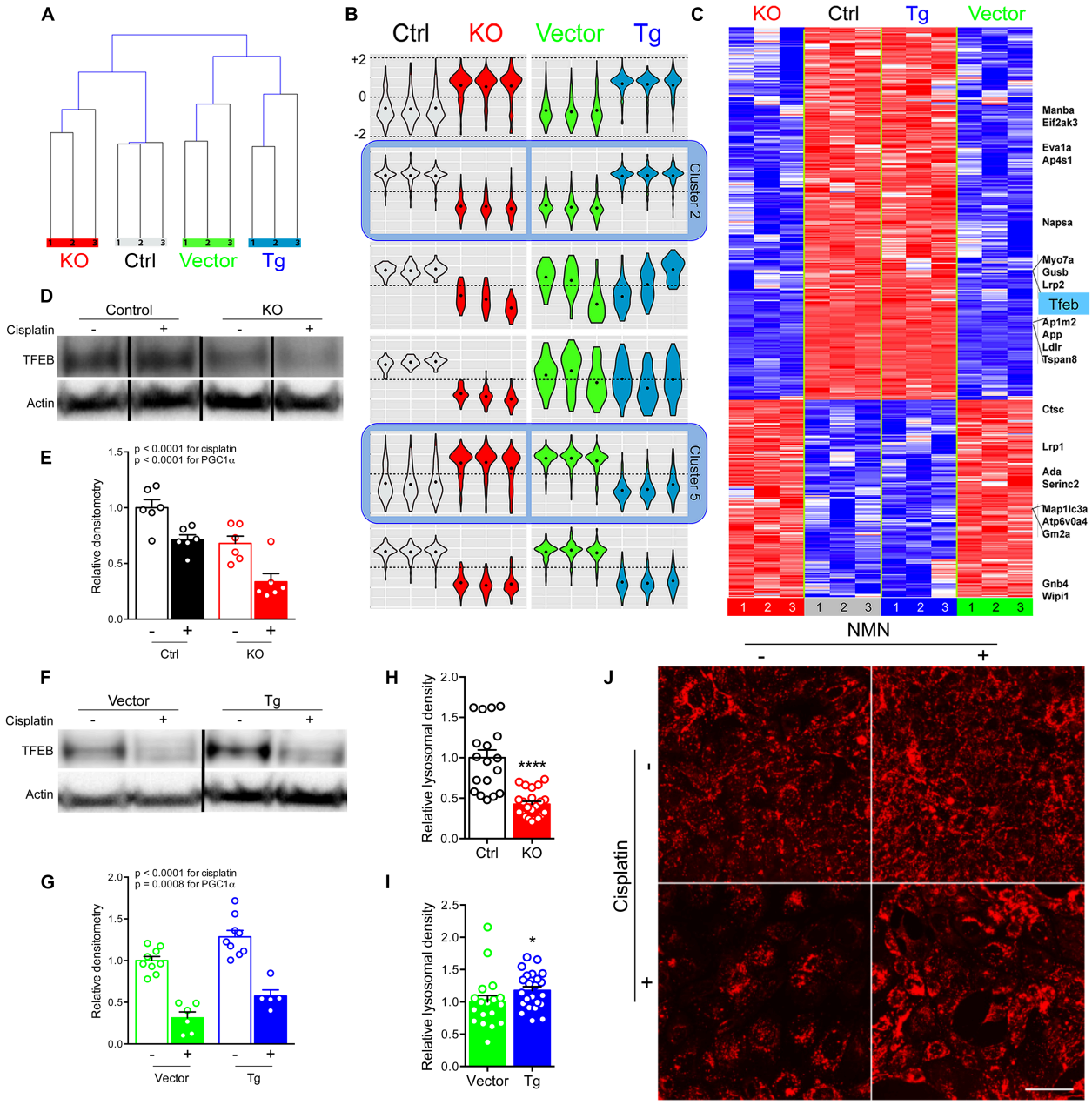


**Figure 4: PGC1α promotes lysosomal biogenesis via TFEB**. (A) Hierarchical clustering of cisplatin-treated (10μM, 24h) PGC1α KO cells or Tg cells and respective controls. (B) Gene expression clusters identified by self-organizing-maps analysis. (C) Heatmap of transcripts in clusters 2 and 5, i.e. oppositely-regulated PGC1α transcripts. (D-G) Representative Western analysis and densitometry of TFEB in cisplatin-treated (10μM, 12h) PGC1α KO cells vs. controls. N=6/condition. (D,E); analogous for PGC1α Tg cells (F,G). N=5-9/condition. P-values as indicated by two-way ANOVA. (H,I) Lysosomal abundance quantified from Lysotracker-stained PGC1α KO (n=18 control vs. 22 KO) or Tg cells (n=18 vector vs. 23 Tg). (J) Representative Lysotracker images (from n=18-24/condition) following cisplatin (10μM, 24h) ± concurrent NMN (1mM). Scale bar 20μm. ****p< 0.0001 by Mann-Whitney.

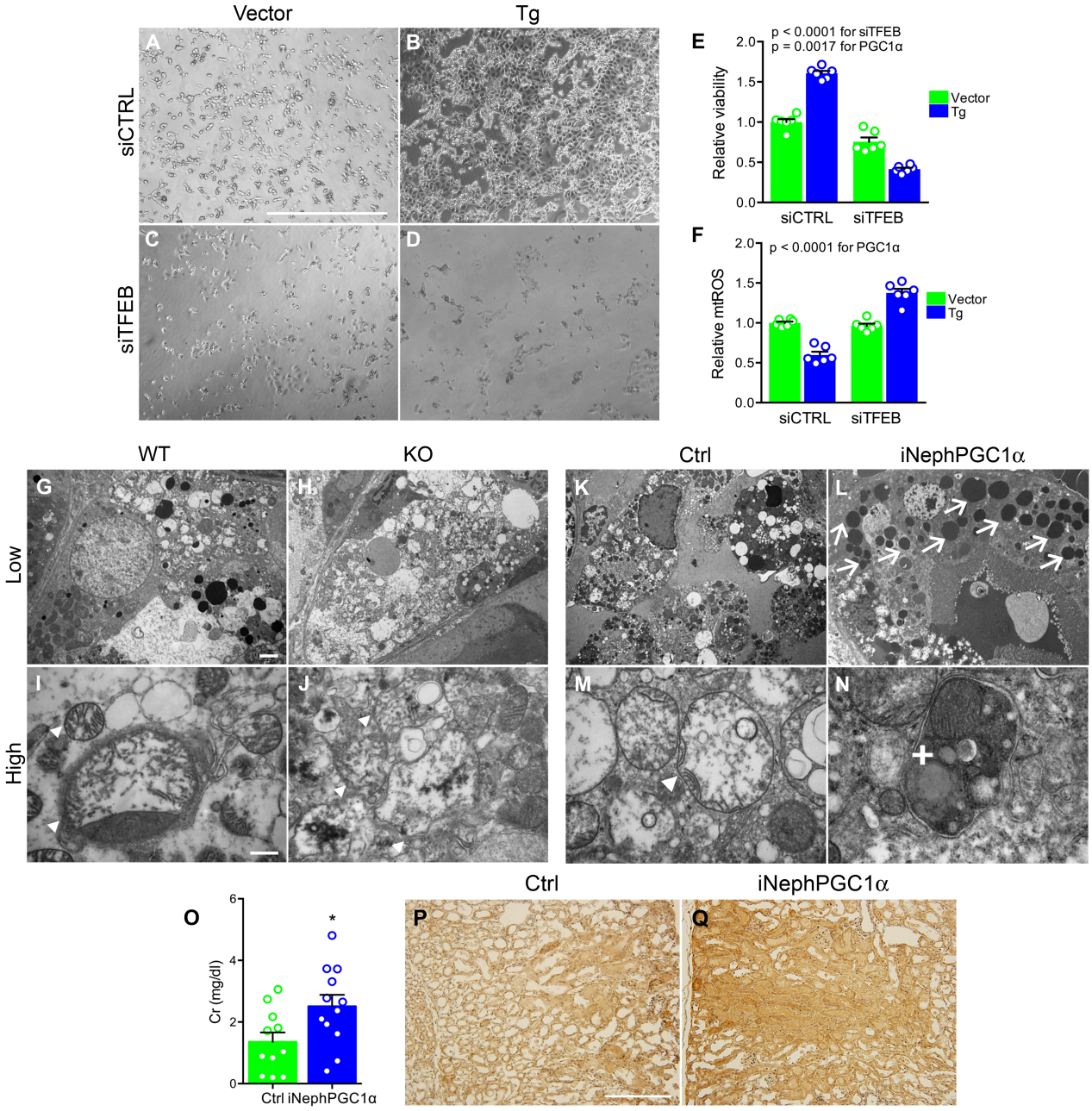


**Figure 5: Lysosomes are pivotal for PGC1α-dependent protection against cisplatin.** (A-D) Representative brightfield images (from n=5/condition) of cisplatin-treated (10μM, 24h) PGC1α Tg cells or vector controls ± TFEB siRNA knockdown (siCTRL or siTFEB, 50μM, 72h). Scale bar 1mm. (E) Viability via XTT assay in (A-D). N=6/condition. (F) Mitochondrial reactive oxygen species (mtROS) via mitoSOX in (A-D). N=6/condition. E and F analyzed by two-way ANOVA. (G-J) Representative low and high-power transmission electron microscopy (TEM, n=3-5 mice/condition) of PGC1α KO or WT proximal tubule 72h after cisplatin (20mg/kg intraperitoneal) showing swollen mitochondria (arrowheads). (K-N) Representative TEM of control or iNephPGC1α proximal tubule 72h after cisplatin (30mg/kg intraperitoneal) showing numerous electron-dense lysosomes (arrows), swollen mitochondria (arrowheads), and a swollen mitochondrion inside a membrane-bound structure consistent with mitophagy (plus sign). Low-power, scale bar 2μm. High-power, scale bar 500nm. (O) Serum creatinine (Cr, mg/dl) in controls (n=11) or iNephPGC1α (n=12 mice) 72h after concurrent cisplatin (30mg/kg intraperitoneal) and chloroquine (10mg/kg intraperitoneal). (P,Q) Representative renal cortex staining (from n=3-5 mice/condition) for 3-nitrotyrosine, a product of oxidative stress, in (O) conditions. Scale bar 200μm. *p<0.05 by Mann-Whitney.